Supporting Information

for

High-Resolution EXAFS Provides Evidence for a Longer Fe•••Fe Distance in the Q Intermediate of Methane Monooxygenase

George E. Cutsail III,[†] Rahul Banerjee, [‡,§] Ang Zhou,[§,#] Lawrence Que, Jr., [§,#] John D. Lipscomb,[‡,§] Serena DeBeer[†,*]

[†]Max Planck Institute for Chemical Energy Conversion, Stiftstr. 34, D-45470 Mülheim an der Ruhr, Germany

[‡]Department of Biochemistry, Molecular Biology and Biophysics, 321 Church St. SE, Minneapolis, MN 55455

[§]Center for Metals in Biocatalysis, University of Minnesota, Minneapolis, Minnesota 55455, USA.

[#]Department of Chemistry, University of Minnesota, 207 Pleasant Street SE, Minneapolis, MN 55455

*Correspondence to: serena.debeer@cec.mpg.de

Fig. S1. Mössbauer spectrum of MMOH^{red} complexed with MMOB collected at 80 K.

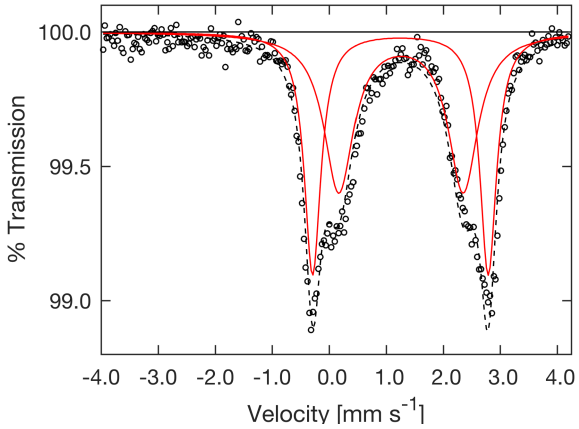

Fig. S2. Mössbauer spectrum of $MMOH^{ox}$ complexed with MMOB collected at 80 K.

A small diiron(II) component (10%), of unoxidized $MMOH^{red}$ is observed and fit as a single quadruple doublet, magenta.

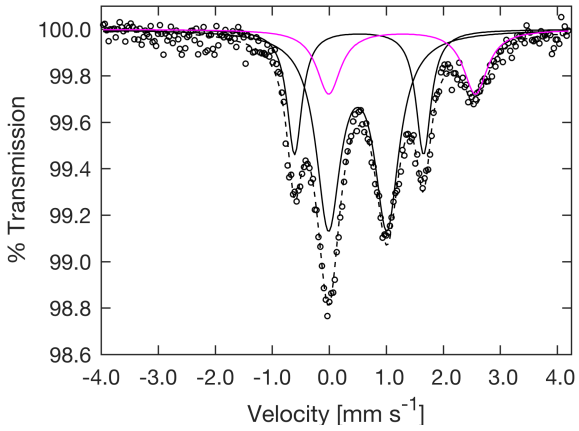

Fig. S3. Mössbauer spectra of MMOH-RFQ (powder packed) collected at 80 K.

Red: $MMOH^{red}$; Black: $MMOH^{ox}$; Blue: MMOH-Q

Sample 1:

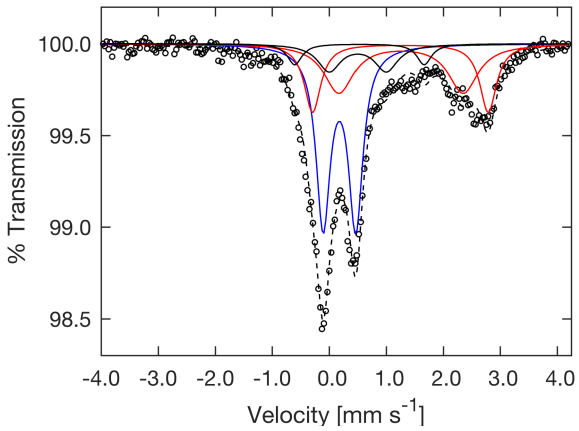

Sample 2:

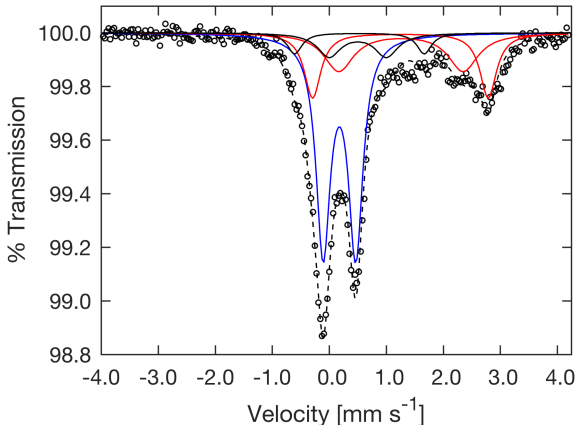

Fig. S4. Mössbauer spectra of MMOH-RFQ (frozen) collected at 80 K.

Red: $MMOH^{red}$; Black: $MMOH^{ox}$; Blue: MMOH-Q

Sample 1:

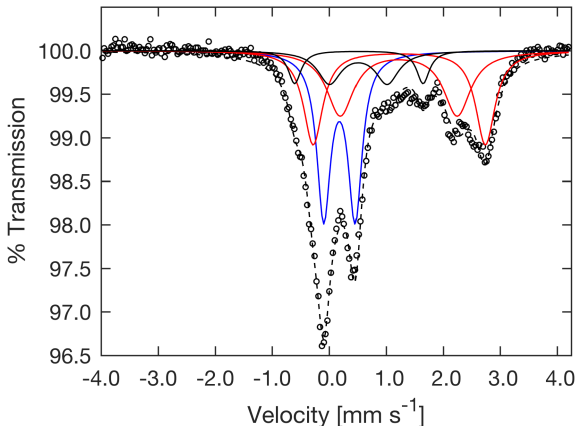

Sample 2:

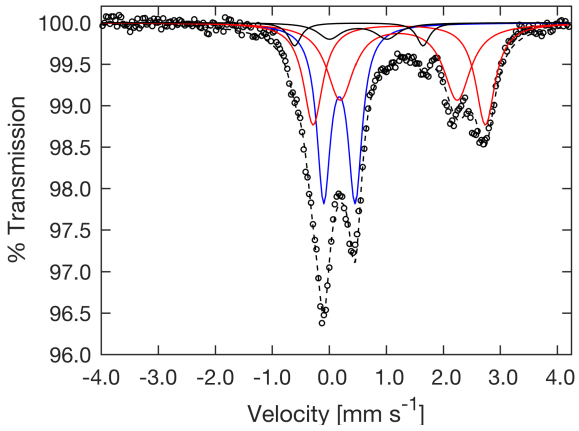

Table S1. Isomer shift (δ) and quadrupole splitting (ΔE_Q) values of the three diiron components within MMOH-RFQ samples.

Isomer shifts and quadrupole splitting experimental values were determine by fitting spectra with Lorentzian lines through the use of the software mf developed by Dr. Eckhard Bill.

	Reduced	**Oxidized**	**Q**	
δ (mm s^{-1})	1.25 1.26	0.53 0.50	0.18	
ΔE_Q (mm s^{-1})	2.18 3.08	2.27 1.00	0.56	
Component %	**39.5** (*36, 43*)	**14.5** (*14, 15*)	**46** (*50, 42*)	**Powder (Fig. S4) (MMOH-RFQ-1)**
	54 (*51*, *57*)	**13** (*17, 9*)	**33.5** (*33, 34*)	**Frozen (Fig. S3) (MMOH-RFQ-2)**

Fig. S5. Kα-HERFD XAS of MMOH^{red}, MMOH^{ox}, MMOH-RFQ, Q and previously published Q.

The 'pure' Q spectrum was obtained by deconvolution of the MMOH-RFQ by subtraction of MMOH^{red} and MMOH^{ox} (complexed with MMOB) based on the Mössbauer quantification (Table S1) compared with the published Kα-HERFD XAS of MMOH-Q from R. G. Castillo, et. al. (Q-RCG). [1]

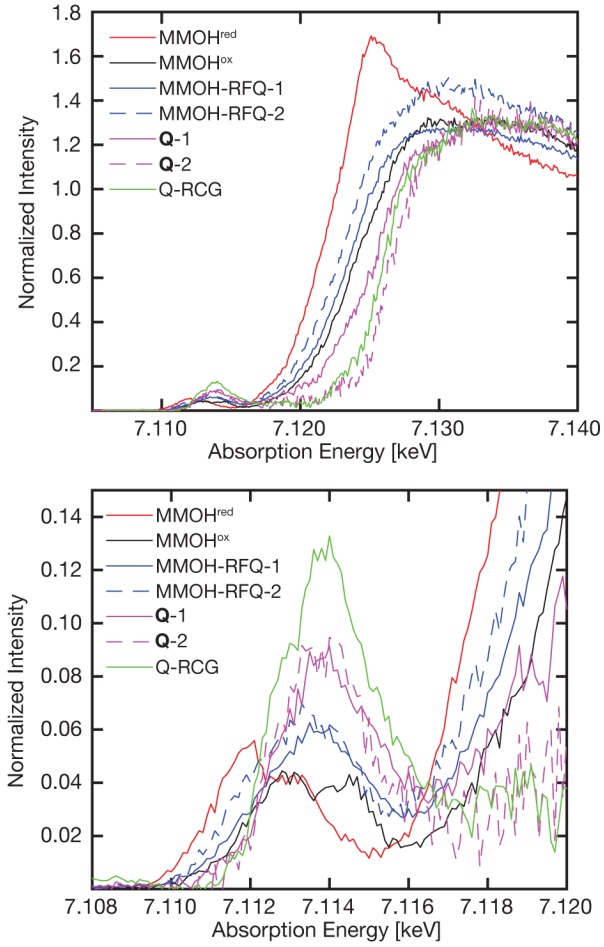

Fig. S6. Fe-Kα emission spectra of $MMOH^{red}$, $MMOH^{ox}$, MMOH-RFQ and MMOH-Q.

The 'pure' MMOH-Q spectrum is the renormalized spectrum of MMOH-RFQ after quantitatively subtraction of the $MMOH^{red}$ and $MMOH^{ox}$ components (complexed with MMOB) based on the Mössbauer quantification. All K α X-ray emission spectra were collected non-resonantly with an incident energy of 7800 eV.

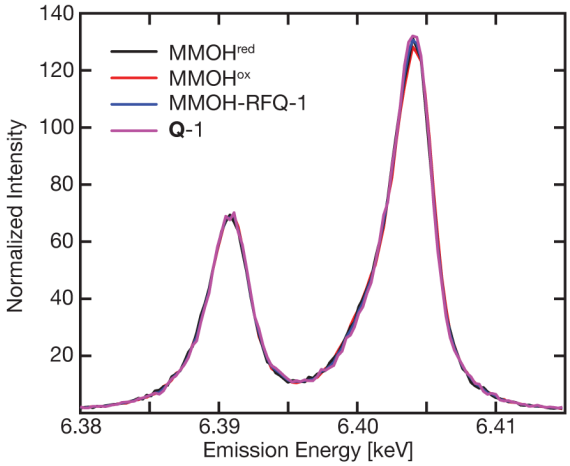

Fig. S7. Kα HERFD-XAS of MMOH-RFQ with digital α-Fe contamination

The edge position of MMOH-RFQ is not dramatically shifted to lower energy upon the addition of ~5% to ~17% α-Fe to the spectrum. However, the pre-edge shape and intensity is strongly modulated. The pre-edge intensity increases over the entire ~7111-7118 eV range, resulting in a pre-edge that is no longer defined by a single peak, but rather a "shelf-like" plateau. This unusual pre-edge shape is the most diagnostic observable in the XAS data for metal contamination.

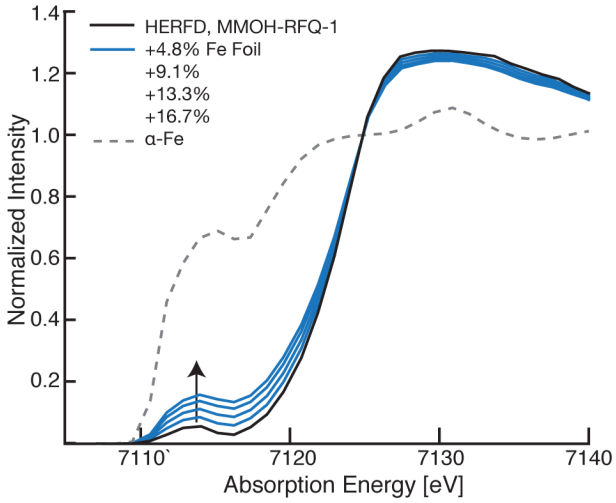

EXAFS fitting.

Theoretical EXAFS spectra were calculated using Artemis[2] utilizing the multiple scattering FEFF6 code.[3] The EXAFS amplitude, $\chi(k)$, is given by

$$\chi(k) = \sum_R S_0^2 N \frac{|\, f_{\text{eff}}(k)\,|}{kR^2} \sin(2kR + \phi_k) \mathrm{e}^{-2kR/\lambda_k} \mathrm{e}^{-2\sigma^2 k^2}$$

where S_0^2 is the overall many-body amplitude factor, N, is the degeneracy of the paths, $|F_{\text{eff}}(k)|$ is the effective scattering amplitude, and R is the absorber-scatterer distance. A Debye-Waller like factor, $\exp(-2\sigma^2 k^2)$ is also included to account for disorder. Lastly, λ_k is the mean free path of the photoelectron and ϕ_k is the total photoelectron wave phase shift for the interaction between the absorber and the scatterer.

Models of $MMOH^{red}$ and $MMOH^{ox}$ were generated from the PDB deposited crystal structures 1FYZ and 1FZ1,[4] respectively, by selection of all atoms within 8 Å of the diiron active site through the use of PyMOL.[5] EXAFS scattering paths were calculated with FEFF6[2] and employed the FEFF cards: SIG2 0.001; RMAX 5; NLEGS 4.

Individual scattering paths were selected and fit within Artemis from paths calculated by FEFF6. The Fourier-transform spectrum of each were fit over a range of R = 1.0 to 3.4 Å (non-phase shift corrected). The FT is the product of a transform of k^3-weighted EXAFS spectrum with a Hann window over the range of $k = 2$ to 11 $Å^{-1}$. By grouping similar scattering paths of a common coordination shell and increasing its degeneracy, N, the number of variables used for that coordination shell is minimal, 2 variables: σ^2 and ΔR. A single ΔE_0 variable is used for all paths in a given fit. S_0^2 was set to 0.9 for all paths. The E_0 for $MMOH^{red}$ and $MMOH^{ox}$ were set to 7122.17 and 7125.12 eV, respectively and MMOH-RFQ-1 and –RFQ-2 samples were 7124.10 and 7123.25 eV, respectively. Goodness of final fits were evaluated by their F-value, defined below:

$$F = \frac{\sum_{i=1}^{n} (d_i - f_i)^2}{\sum_{i=1}^{n} {d_i}^2}$$

where d and f represent the raw data and the fit, respectively. All reported F-values were calculated over an expanded R range of R = 0 to 4 Å.

Fig. S8. Additional HERFD-EXAFS fits of MMOH^{ox}

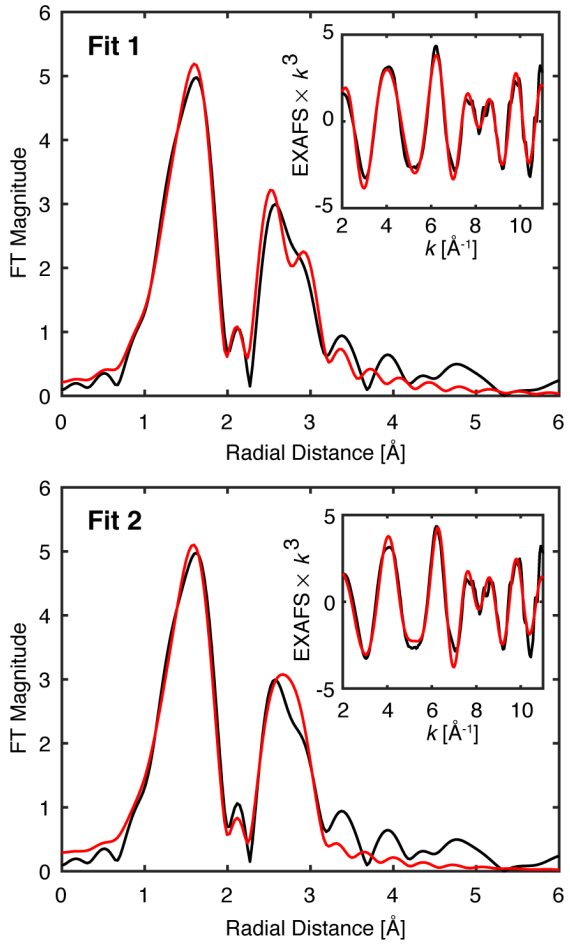

Table S2. HERFD-EXAFS Fit Parameters of MMOH^{ox} for Fig. S8

Fit 1					
N	**Scattering Path**	**R (Å)**	**+/–**	**σ^2 ($\times 10^{-3}$ Å^2)**	**+/–**
5	Fe-O/N	2.057	0.010	12.6	1.0
1	Fe-O/N	2.480	0.036	9.9	5.7
1	Fe-Fe	3.056	0.011	1.3	0.9
3	Fe-C	3.304	0.031	4.9	4.1
ΔE_0 = + 2.51 eV				F = 0.163	
Fit 2					
5	Fe-O/N	2.053	0.014	12.4	1.2
1	Fe-O/N	2.470	0.043	9.9	6.8
1	Fe-Fe	3.048	0.012	2.5	0.9
ΔE_0 = + 1.75 eV				F = 0.184	

Fig. S9. Comparison of PFY MMOH^{red} with phase-shift recorrection.

FT-EXAFS comparisons of HERFD-MMOH^{red} with the previously published PFY-MMOHred from Shu, et al, subtracting the reported 0.35 Å phase-shift (top panel), with a subtraction of 0.50 Å phase-shift.

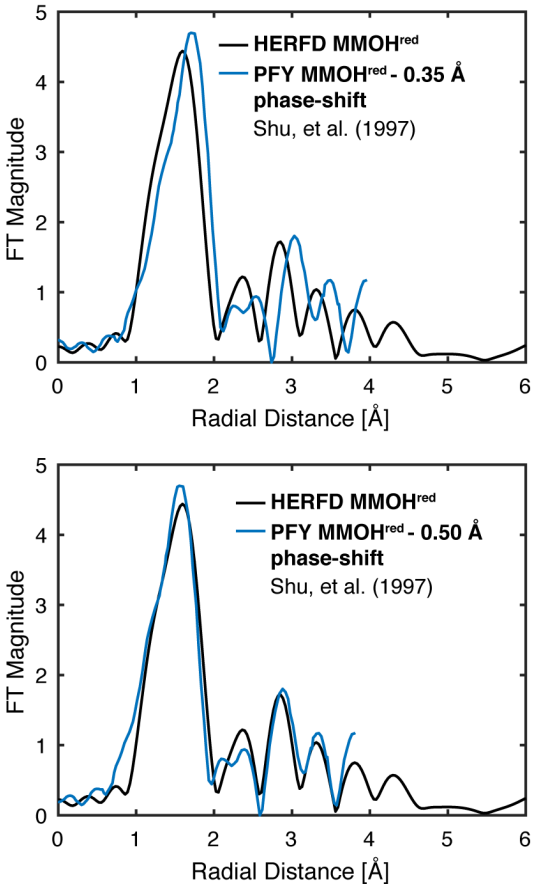

Fig. S10. Additional HERFD-EXAFS fits of MMOH^{red}

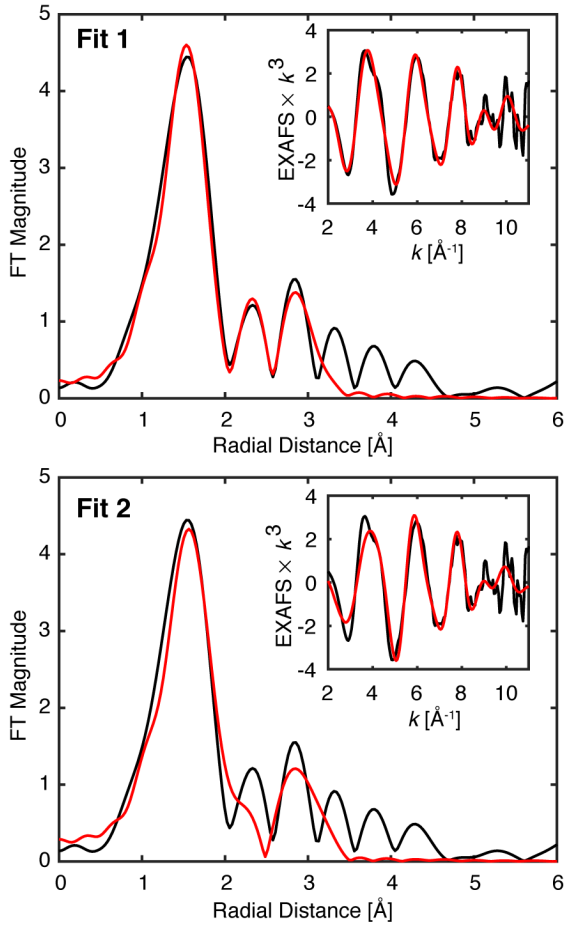

Table S3. HERFD-EXAFS Fit Parameters of MMOH^{red} for Fig. S10

Fit 1					
N	**Scattering Path**	**R (Å)**	**+/–**	**σ^2 ($\times 10^{-3}$ Å^2)**	**+/–**
4	Fe-O/N	2.044	0.015	10.3	1.1
1	Fe-O/N	2.538	0.022	2.6	2.6
1	Fe-Fe	3.270	0.026	8.4	2.5
3	Fe-C	2.989	0.051	20.0	8.0
ΔE_0 = –6.63 eV				F = 0.489	
Fit 2					
4	Fe-O/N	2.062	0.026	10.3	1.5
1	Fe-O/N	2.542	0.035	3.7	4.2
1	Fe-Fe	3.306	0.041	9.2	4.1
ΔE_0 = –4.001 eV				F = 0.683	

Table S4. HERFD-EXAFS Fit Parameters of MMOH-RFQ (Attempts to fit short diiron distance ~ 2.8 Å).

Fit A					
MMOH-RFQ HERFD – 1					
N	**Scattering Path**	**R (Å)**	**+/–**	**σ^2 ($\times 10^{-3}$ Å^2)**	**+/–**
5	Fe-O/N	2.053	0.016	13.7	1.2
1	Fe-O/N	1.780	0.020	7.5	2.4
0.5	Fe-Fe	2.668	0.040	14.6	5.4
0.5	Fe-Fe	3.385	0.020	3.0	2.1
ΔE_0 = -2.002 eV				F = 0.41487	
MMOH-RFQ HERFD – 2					
5	Fe-O/N	2.035	0.015	12.0	1.0
1	Fe-O/N	1.759	0.018	7.14	2.4
0.5	Fe-Fe	2.649	0.051	16.7	7.2
0.5	Fe-Fe	3.337	0.016	1.34	1.5
ΔE_0 = -4.186 eV				F = 0.28673	
Best Fit (as shown in Fig. 10, Table 3)					
MMOH-RFQ HERFD – 1					
N	**Scattering Path**	**R (Å)**	**+/–**	**σ^2 ($\times 10^{-3}$ Å^2)**	**+/–**
1	Fe-O	1.781	0.018	8.3	2.3
5	Fe-O/N	2.057	0.014	13.8	1.0
0.3	Fe-Fe	3.067	0.025	1.9	2.4
0.7	Fe-Fe	3.343	0.030	8.0	4.2
ΔE_0 = -1.454 eV				F = 0.35461	
MMOH-RFQ HERFD – 2					
1	Fe-O	1.758	0.011	7.6	1.5
5	Fe-O/N	2.035	0.009	12.1	0.6
0.3	Fe-Fe	3.053	0.019	1.2	1.8
0.7	Fe-Fe	3.303	0.015	3.7	1.6
ΔE_0 = -4.060 eV				F = 0.20059	

Fig. S11. HERFD-EXAFS fits of MMOH-RFQ – 1 and 2, as Detailed in Table S4.

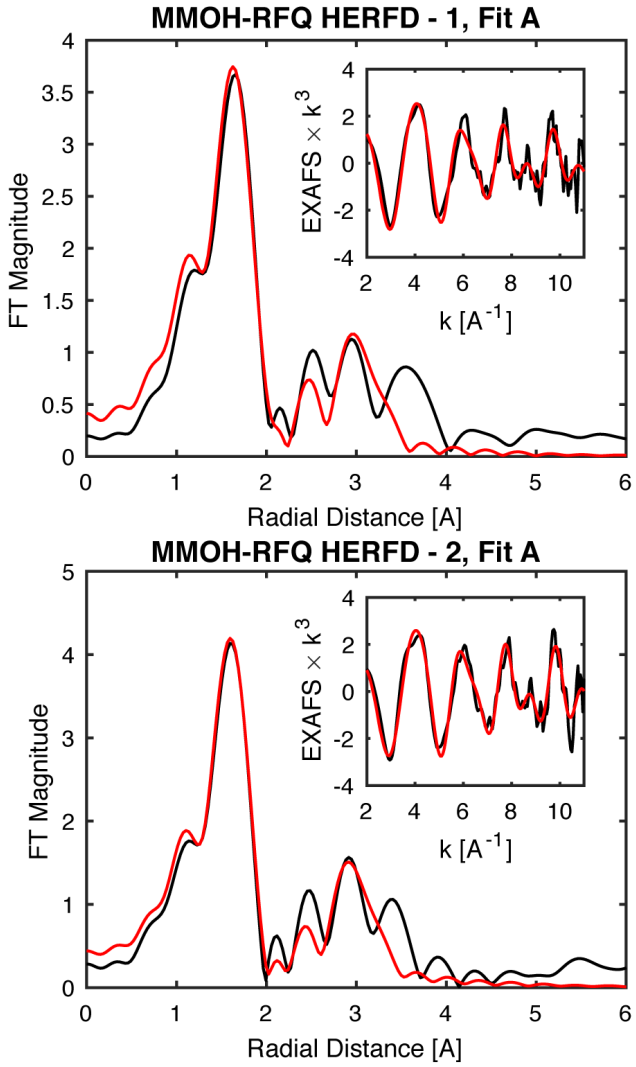

1. Castillo, R. G.; Banerjee, R.; Allpress, C. J.; Rohde, G. T.; Bill, E.; Que, L.; Lipscomb, J. D.; DeBeer, S., High-energy-resolution fluorescence-detected x-ray absorption of the Q intermediate of soluble methane monooxygenase. *J. Am. Chem. Soc.* **2017,** *139* (49), 18024-18033.
2. Ravel, B.; Newville, M., ATHENA, ARTEMIS, HEPHAESTUS: data analysis for X-ray absorption spectroscopy using IFEFFIT. *J. of Synchrotron Rad.* **2005,** *12* (4), 537-541.
3. Zabinsky, S. I.; Rehr, J. J.; Ankudinov, A.; Albers, R. C.; Eller, M. J., Multiple-scattering calculations of X-ray-absorption spectra. *Phys. Rev. B: Condens. Matter Mater. Phys.* **1995,** *52* (4), 2995-3009.
4. Whittington, D. A.; Lippard, S. J., Crystal structures of the soluble methane monooxygenase hydroxylase from *Methylococcus capsulatus* (Bath) demonstrating geometrical variability at the dinuclear iron active site. *J. Am. Chem. Soc.* **2001,** *123* (5), 827-838.
5. The PyMOL Molecular Graphics System, Version 1.8. **2015**.